Chemical Engineering Research and Design 194 (2023) 121–135

Available online at www.sciencedirect.com

Chemical Engineering Research and Design

journal homepage: www.elsevier.com/locate/cherd

Modeling and performance analysis of electrostatic desalter using combined CFD-PBM method

Mohammad Rahmani[a], *Nassim Tahouni*[a,*], *Mojgan Abbasi*[b], *M. Hassan Panjeshahi*[a]

[a] *School of Chemical Engineering, College of Engineering, University of Tehran, Tehran, Iran*

[b] *Institute of Petroleum Engineering, School of Chemical Engineering, College of Engineering, University of Tehran, Tehran, Iran*

ARTICLE INFO

Article history:
Received 19 January 2023
Received in revised form 12 April 2023
Accepted 14 April 2023
Available online 17 April 2023

Keywords:
Electrostatic desalter
Computational fluid dynamics
Population balance model
Electric field

ABSTRACT

In this research, a combined method of computational fluid dynamics and population balance model were used to simulate the electrostatic desalter units using the ANSYS Fluent software. The goal of this study is to investigate the effective parameters in separating brine from oil and optimizing the desalter performance. The model was subjected to sensitivity analysis for four parameters: temperature, wash water percentage, inlet distributor, and electrodes arrangements. The results showed that raising the temperature up to 130 °C and increasing the wash water percentage improved the separation. Also, the separation is greatly improved by switching to a T-shaped input distributor. The separation is not considerably affected by the number of horizontal electrodes, while the vertical electrodes have a negative impact. Finally, sensitivity analysis was performed on an existing desalter located in one of the Iran's oil fields. The findings demonstrated that the current situation does not meet the acceptable limit of 0.3% vol of brine in the oil outlet. The desalter outlet meet the specifications by switching the type of distributor to a T-shaped one, and additionally when the temperature is 90 °C and 10% wash water or 100 °C and 8.3% wash water without changing the geometry.

1. Introduction

Since crude oil contains water and the majority of its salt dissolves in small drops of water; removing water also eliminates salt from crude oil. This water often contains soluble salts, including calcium, magnesium, and sodium chloride. The equivalent of sodium chloride in parts per million is how much salt is in a given volume of water (Arnold and Stewart, 2008). The salt concentration in crude oil-produced water in Iran's oil fields is 150,000–220,000 ppm (52576–77112 pounds of salt per thousand barrels of crude oil (PTB)) (Zeidani and Bahadori, 2008).

Oil containing salt typically clogs downstream processing equipment and deactivates catalyst beds. Because of these issues, refineries usually require that the crude oil 's concentration be drastically reduced before processing. Salt is typically specified at 10–20 PTB (Arnold and Stewart, 2008).

Oil desalination is the process of removing water-soluble salts from the oil stream. The best desalination devices remove as much water as possible. Any device that removes water from the oil can be used as a desalter (Arnold and Stewart, 2008). Desalination methods include settling, chemical, thermal, mechanical, and electrical coalescing (Sadatshojaie et al., 2021). Most of the used desalters are

* Corresponding author.
E-mail address: ntahuni@ut.ac.ir (N. Tahouni).

https://doi.org/10.1016/j.cherd.2023.04.033

Nomenclature

AC	alternating current.
CFD	computational fluid dynamics.
FAVEG	facet average of velocity in the entire geometry (m/s).
FAVFWOO	facet average of volume fraction of water at oil outlet.
FAVOO	facet average of velocity at oil outlet (m/s).
IOFD	Iran's oil field desalter.
PBM	population balance model.
PTB	pounds of salt per thousand barrels of crude oil.
RAD	Ramirez-Argaez et al., 2021 desalter.
RAM	Ramirez-Argaez et al., 2021 method.
UDF	user-defined function.

Symbols

$a(d_i, d_j)$	Aggregation rate, s^{-1}.
c	Molar concentration of equivalent NaCl, g-moles/Lit.
d	Droplet diameter, m.
d_{32}	Sauter mean diameter.
E	Electric field, V/m.
F	Body force, N.
f	Class fraction.
G	Generation of turbulence kinetic energy, $J/(m^3.s)$.
g	Gravitational acceleration, m/s^2.
$g(d_i)$	Breakage frequency, 1/s.
$K(d_i, d_j)$	Coalescence rate due to electrostatic force, s^{-1}.
k	Kinetic energy of turbulence, J/kg.
n	The average number of droplets per unit volume, m^{-3}.
P	Pressure, Pa.
$P(d_i, d_j)$	Coalescence probability.
q_v	Volumetric charge density, C/m^3.
q'	Ratio factor.
Re	Reynolds number.
T	Temperature, K.
We	Weber number.

Greek symbols

α	volume fraction.
$\beta(d_i \mid d_j)$	probability density function.
ε	turbulence dissipation rate, m^2/s^3.
ε'	absolute permittivity, F/m.
λ	electrical conductivity, S/m.
μ	viscosity, Pa.s.
ν	velocity, m/s.
ν_{dr}	drift velocity, m/s.
ξ	eddy dimensionless size.
ρ	density, kg/m^3.
σ'	interfacial tension, N/m.
φ	electric potential, V.
$\omega(d_i, d_j)$	coalescence frequency, 1/s.
$\Omega_{br}(d_i, d_j)$	breakage rate, 1/s.

Subscript

b	brine.
m	mixture.
o	oil.
t	turbulence.
w	water.

horizontal electrostatic treaters. These treaters produce the lowest level of residual water compared to other treaters (Arnold and Stewart, 2008).

To model electrostatic desalters, researchers have used different methods. Al-Otaibi et al. (2005) developed an artificial neural network as a modeling method to simulate and optimize the desalination/dehydration process system. The efficiency of salinity and water cut, which is predicted to depend on the concentrations of emulsifiers, heating, wash water, salt concentration, and the amount of mixing with wash water, was calculated in their study to assess the effectiveness of the desalination/dehydration process. Neural network model predictions are compared with actual observations and consistency is shown in the results. Then the prepared neural network model is used to optimize the performance. Kiani et al. (2013) used artificial neural networks to model the efficiency of the desalination unit as a function of the input parameters. The findings of this study showed that the model matches the experimental data.

Meidanshahi et al. (2012) introduced a new mathematical model based on the two-variable population balance equation to simulate the steady state distribution of water droplet size and salt concentration in an alternating current (AC) electrostatic desalter. The effect of different operating parameters on crude oil salt content and output dehydration efficiency was studied. In addition, the effect of the two-stage desalter on the output of basic sediments and water and the amount of salt in oil was investigated. To achieve the optimum electrostatic desalter performance, the parameters of this model was improved using the differential evolutionary technique. The results demonstrated that the proposed model can be effectively used to study the impact of different parameters on the AC electrostatic desalter performance in separating water from crude oil emulsions. Aryafard et al. (2016) developed a mathematical model to predict water and salt separation efficiency in a two-stage industrial process for crude oil desalting. The considered process includes a mixing valve and electrostatic desalter that are connected in series. The desalter unit is modeled based on the population balance method by considering the breaking and coalescence of water drops to predict the droplet size distribution. The class method is chosen as a common mathematical method to solve the population balance equation. The accuracy of the extended mathematical model and the assumed assumption was evaluated using the data from an industrial desalter unit. Then, the effect of mixing valve pressure drops, wash water flow rate, and electric field strength on desalination and dehydration efficiency was investigated. According to the simulation results, increasing the wash water flow rate from 3% to 6% reduces the amount of salt in treated crude oil from 2.06 to 0.71 PTB. By considering a partial circuit model in the coagulation vessel, Kakhki et al. (2016) used the population balance equation to describe a dewatering process including a mixing valve and an electrostatic coagulation vessel. Electrode plates and crude oil emulsion are considered as capacitors and insulating materials, respectively. Based on the proposed model, it is explored how temperature, wash water rate, and current frequency effect the applied electric field strength, breakage voltage, water droplet size distribution, and output water amount in treated crude oil. According to the simulation results, increasing the current frequency from 50 to 300 Hz reduces the amount of water in treated crude oil from 0.12% to 0.09%. Roshan et al. (2017) presented a theoretical model to investigate the effect of demulsifier agents on the efficiency of water separation from crude oil emulsion. A relationship between the critical concentration of demulsifier agents and the collision frequency function in the population balance equation was presented using thermodynamic balance principles. The comparison of simulation and laboratory results showed the model suitability in predicting the separation efficiency of water droplets from crude oil emulsion in different demulsifier agent concentrations. Khajehesamedini et al. (2018) proposed a laboratory setup to investigate the possibility of using low-frequency ultrasonic waves as an alternative to reduce the consumption of chemical demulsifiers in the pretreatment of crude oil. These experiments were designed to study the effects of irradiation duration, ultrasonic field intensity, and the initial amount of water on separation efficiency. In addition, a population balance model (PBM) was presented to explain the experimental data. A hybrid model was developed to determine the frequency of droplet aggregation. Model parameters were estimated by linear regression. Parameter estimation was done using the parallel implementation of the particle swarm optimization algorithm. The model's output revealed a reasonable agreement with the laboratory data.

Oshinowo et al. (2016) used a laboratory approach and numerical modeling to evaluate the separation of a water-in-oil emulsion in a batch gravity separator. The separation behavior of crude oil emulsions was simulated using multiphase computational fluid dynamics (CFD) with a population balance model. The class method is used to solve population balance equations. To explain how emulsion viscosity rises with water concentration, an emulsion viscosity model was chosen. The results of the CFD code were compared with the laboratory data. The time-dependent profiles of the water fraction in the separator were in good agreement with the laboratory measurements for the range of water content from 6% to 50%. This model predicts the effect of water fraction on the separation speed. Thaker and Buwa (2020) have developed a multi-fluid Eulerian CFD model Using OpenFOAM software, that includes binary and interfacial coalescence processes. The separation of kerosene dispersed in water is simulated in a batch separator and validated by measuring the coalescence completion time, the volume fraction of the dispersed phase, and the droplet size distribution. While using the two-fluid model with modified drag experimental relations, the time of coalescence completion can be well predicted, but the volume fraction of the dispersed phase and the droplet size distribution cannot be predicted. It is shown that the comprehensive multi-fluid Eulerian model, which includes binary and interfacial coalescence, predicts the coalescence completion time, the volume fraction of the dispersed phase, and the droplet size distribution in excellent agreement with the measurements.

Ramirez-Argaez et al. (2021) studied the desalination process using the collision time of two drops in a water-in-oil emulsion based on force balance. First, the model was numerically solved, and a process analysis was performed to determine the effect of the main process' key variables, such as the strength of the electric field, water amount, temperature, and droplet size on collision frequency between a pair of droplets. Then, by using the calculated collision frequency, the correlations related to the "interfacial area concentration" method were modified in the ANSYS Fluent software and the desalination process was compared in the presence and absence of the electric field.

Tahouni et al. (2023) improved the performance of a crude oil treatment unit and maximized the oil production. The process involves a two-stage desalting unit followed by a stabilizer tower. They modeled the desalting process using the population balance equation in MATLAB and then simulated the whole process by linking the numerical code and a simulator. In their research, the desalting and stabilization units were simultaneously optimized due to the existing interactions between the desalters and the stabilizer tower.

In this study, the population balance model is used to model the behavior of brine droplets. The computational fluid dynamics method is used to study the behavior of crude oil, which is a continuous phase. By combining these two methods and using ANSYS Fluent software, the interaction between phases and, as a result, the performance of an electrostatic desalter is simulated. The innovation of this work is to calculate the electric field value with solving charge conservation equation by using User Defined Function (UDF) in Ansys Fluent and apply its effect in the momentum and population balance equations.

2. Mathematical modeling

2.1. Assumptions

The assumptions used in the modelling of a desalter are as follows:

- The system is isothermal, meaning there is no temperature change.
- Each phase is a Newtonian and incompressible fluid with fixed physical properties.
- Equations are solved in steady-state conditions.
- Crude oil is regarded as a continuous primary phase and brine is a dispersed secondary phase.
- Only binary coalescence and breakage are considered
- Droplet breakage in the electric field is neglected.
- Spherical droplets are assumed.

2.2. Governing equations

The mixture approach is used to model the multi-phase system that solves a single set of equations: Continuity equation, Navier-Stokes momentum equations, and k-ε realizable turbulence model. It has recently been applied in many complex flow systems and has the best convergence behavior. The mixture model calculates the density, viscosity, and velocity of the mixture based on the volume fraction composition of the mixture in each cell (Ramirez-Argaez et al., 2021).

Eqs. (1) and (2) provide the continuity and momentum equations for this model (ANSYS, 2019):

$$\nabla.\,(\rho_m \vec{v}_m) = 0 \quad (1)$$

$$\nabla.\,(\rho_m \vec{v}_m \vec{v}_m) = -\nabla P + \nabla.\,[(\mu_m + \mu_t)(\nabla \vec{v}_m + \nabla \vec{v}_m^{\,T})] + \rho_m \vec{g} + \vec{F} + \vec{F}_e - \nabla.\,(\textstyle\sum_{k=1}^{n} \alpha_k \rho_k \vec{v}_{dr,k} \vec{v}_{dr,k}) \quad (2)$$

where $\vec{v}_m$ is the mass-averaged velocity, ρ_m is the mixture density, P is the pressure, μ_m is the mixture viscosity, μ_t is the turbulent viscosity, α_k is the volume fraction of phase k, $\vec{v}_{dr,k}$ is the drift velocity for secondary phase k, $\vec{F}$ is a body force, $\vec{F}_e$ is the electrostatic force.

Eqs. (3) and (4) state the turbulent transport equations in the realizable k-ε model (ANSYS, 2019):

$$\frac{\partial}{\partial x_j}(\rho_m k v_{m,j}) = \frac{\partial}{\partial x_j}\left[\left(\mu_m + \frac{\mu_t}{\sigma_k}\right)\frac{\partial k}{\partial x_j}\right] + G_k + G_b - \rho_m \varepsilon - Y_M \tag{3}$$

$$\frac{\partial}{\partial x_j}(\rho_m \varepsilon v_{m,j}) = \frac{\partial}{\partial x_j}\left[\left(\mu_m + \frac{\mu_t}{\sigma_\varepsilon}\right)\frac{\partial \varepsilon}{\partial x_j}\right] + \rho_m C_1 S\varepsilon - \rho_m C_2 \frac{\varepsilon^2}{k + \sqrt{\nu\varepsilon}} + C_{1\varepsilon}\frac{\varepsilon}{k}C_{3\varepsilon}G_b \tag{4}$$

where k is the kinetic energy of turbulence, ε is the turbulence dissipation rate, G_k is the generation of turbulence kinetic energy due to the mean velocity gradients, G_b is the generation of turbulence kinetic energy due to buoyancy, Y_M is the contribution of the fluctuating dilatation in compressible turbulence to the overall dissipation rate, and $C_{1\varepsilon}$, C_2, σ_k, and σ_ε are constants and are equal to 1.44, 1.9, 1.0, and 1.2 respectively.

Because the brine-in-oil emulsion is a leaky dielectric fluid, its electrical conductivity is limited and electrostatic charges accumulate at the interface of two phases. Due to the leaky dielectric emulsion and the associated simplifying assumptions, Eq. (5), the charge conservation equation, governs the system and accounts for the presence of an electric field (Rahmat, 2017):

$$\nabla.(\lambda_m \nabla\varphi) = 0 \tag{5}$$

where λ_m is the mixture's electrical conductivity and φ is the electric potential. After solving this equation, the electric potential is determined. By using electric potential, it is possible to calculate the electric field distribution and then the electrostatic force on the fluid (Rahmat, 2017):

$$\vec{E} = -\nabla\varphi \tag{6}$$

$$\vec{F_e} = \nabla.(\varepsilon'_m \vec{E})\vec{E} - 0.5\vec{E}.\vec{E}\nabla\varepsilon'_m \tag{7}$$

where $\vec{E}$ is the electric field and ε'_m is the mixture's absolute permittivity.

The population balance equation (Eq. 8) is used to account for droplets coalescence and breakage due to electrostatic and turbulence effects to calculate the droplet diameter distribution (Aryafard et al., 2016):

$$v\frac{\partial n(d_i, z)}{\partial z} = \frac{1}{2}\int_0^{d_i} a(d_i - d_j, d_j)n(d_i - d_j, z)n(d_j, z)dd_j - \int_0^{\infty} a(d_i, d_j)n(d_i, z)n(d_j, z)dd_j + \int_{\Omega_d} pg(d_j)\beta(d_i|d_j)n(d_j, z)dd_j - g(d_i)n(d_i, z) \tag{8}$$

where ν is the velocity, d is the droplet diameter, $n(d_i, z)$ is the average number of droplets per unit volume that have diameter d_i at position z, $a(d_i, d_j)$ is the aggregation rate, $g(d_i)$ is the breakage frequency, and $\beta(d_i \mid d_j)$ is the probability density function of the formation of a droplet with a diameter d_i from the breakage of a droplet with a diameter d_j, and p is the number of particles produced as a result of breakage (which is equal to 2 in binary breakage). The first and second expressions on the right side of the equation show the birth and death of droplets due to coalescence, while the third and fourth expressions show the birth and death of droplets due to breakage.

The coalescence rate in an electrostatic desalter is divided into two parts (Gong et al., 2021) according to Eq. (9). The first part is related to the hydrodynamic effect (Wang et al., 2005) and the second part is related to the electrostatic effect (Atten, 1993):

$$a(d_i, d_j) = \omega(d_i, d_j)P(d_i, d_j) + K(d_i, d_j) \tag{9}$$

where $\omega(d_i, d_j)$ is the coalescence frequency, $P(d_i, d_j)$ is the coalescence probability, and $K(d_i, d_j)$ is the coalescence rate due to electrostatic force where calculate from Eqs. (10) to (12), respectively.

$$\omega(d_i, d_j) = \frac{\pi\sqrt{2}}{4}\varepsilon^{1/3}(d_i + d_j)^2(d_i^{2/3} + d_j^{2/3})^{1/2} \tag{10}$$

$$P(d_i, d_j) = \exp\left\{-\frac{[0.75(1 + (d_i/d_j)^2)(1 + (d_i/d_j)^3)]^{1/2}}{(\rho_b/\rho_o + 0.5)^{1/2}(1 + d_i/d_j)^3}We_{ij}^{1/2}\right\} \tag{11}$$

$$K(d_i, d_j) = \frac{2\pi}{9}(d_i + d_j)^3\left(\frac{d_i}{d_j} + \frac{d_j}{d_i}\right)\left(\frac{\varepsilon'_o E^2}{\mu_o}\right) \tag{12}$$

where ρ_b and ρ_o are the brine and oil density, ε'_o is the oil's absolute permittivity, μ_o is the oil viscosity, and We is the Weber number calculated from Eq. (13).

$$We_{ij} = \frac{\sqrt{2}}{\sigma'}\rho_o d_i \varepsilon^{1/3}(d_i^{2/3} + d_j^{2/3})^{1/2} \tag{13}$$

where σ' is the interfacial tension.

The breakage rate is calculated using the Luo and Svendsen, 1996 model (Eq. 14), which includes the breakage frequency and the probability density function of droplet formation:

$$\Omega_{br}(d_i, d_j) = 0.9238\varepsilon^{1/3}d_j^{-2/3}\alpha\int_{\xi_{min}}^{1}\frac{(1+\xi)^2}{\xi^{11/3}}\exp\left(-\frac{1.52\sigma'\xi^{-11/3}}{\rho_o\varepsilon^{2/3}d_j^{5/3}}\right)d\xi \tag{14}$$

where ξ and ξ_{min} are the eddy dimensionless size and the minimum eddy dimensionless size, respectively.

The Sauter mean diameter (equation 15) is calculated and used to represent the droplet diameter from the population balance equation, then transferred to the conservation equations and corrected the interphase force, so that relevant flow properties such as velocity and volume fraction of the dispersed phase are calculated and updated.

$$d_{32} = \frac{\sum n_i d_i^3}{\sum n_i d_i^2} \tag{15}$$

where n_i is the number of class i droplets per unit volume.

3. Simulation

The electrostatic desalter's performance is simulated using ANSYS Fluent software. The charge conservation equation is added to the software via UDFs. After calculating the voltage distribution in the desalter, the resulting electric field is calculated. UDFs are also used for applying the electric field effect on the momentum and population balance equations.

3.1. *Geometry*

The geometry of the desalter is drawn using SpaceClaim software. In this study, two dimensions are used for the desalter shown in Table 1. Fig. 1(a) and (b) depict, respectively, the chosen desalter geometry from the Ramirez-Argaez et al.,

Table 1 – Desalters dimensions.

	Ramirez-Argaez et al. (2021) 's desalter (RAD)	Iran's oil field desalter (IOFD)
Length (m)	15.44	30
Diameter (m)	3.66	4.8
Electrodes Distance (m)	0.32	0.32

2021 article (case study I) and from an oil filed in Iran (case study II).

3.2. *Boundary conditions*

In an electrostatic desalter, there are electric field effects in addition to fluid flow. For this reason, we have two types of boundary conditions: hydrodynamic and electrostatic. The boundary conditions used in the simulation are described in Table 2.

Due to the unavailability of experimental data, Eqs. (16) to (19) are used to calculate the minimum / maximum diameter and size distribution of brine droplets at the inlet (Oshinowo et al., 2015):

$$d_{\min} = \frac{8\sigma'}{g\rho_o u_o^2} \quad (16)$$

$$d_{\max} = \frac{0.725}{(\rho_o/\sigma')^{3/5}\varepsilon^{2/5}} \quad (17)$$

$$q' = \frac{3\ln(d_2/d_1)}{\ln 2} = \frac{3\ln(d_{i+1}/d_i)}{\ln 2} = \frac{3}{N-1}\frac{\ln(d_{\max}/d_{\min})}{\ln 2} \quad (18)$$

$$f_i = 1 - \exp\left(-\left(\frac{d_i}{0.4d_{\max}}\right)^2\right) \quad (19)$$

where d_{min} and d_{max} is are minimum and maximum droplets number, d_i is the droplets diameter in the i^{th} class, q' is the ratio factor, N is the number of classes, and f_i is the i^{th} class fraction.

The ratio factor is calculated using the minimum and maximum droplets diameter. The number of classes determines the class droplet diameter, and the droplet diameter in each class reveals the class fraction.

3.3. *Method for solving equations*

The coupled scheme is used for pressure-velocity coupling, and the first-order upwind discretization method is used to solve the momentum and turbulence equations. Population balance equations are solved using the discretization method or class method. The first-order upwind discretization method is used to solve the equations associated with each class.

3.4. *Operating conditions and physical properties*

The operating conditions and physical properties used in RAD and IOFD simulation are listed in Table 3 and, respectively.

Empirical equations and charts are used to calculate physical properties at different temperatures.

- brine density (Dittman, 1977):

$$\rho_b = 17.655a_3 - 28.89a_2T + 7373.37a_2 \quad (20)$$

where T is the temperature in K, ρ_b is the brine density in kg/m^3, and a_2 and a_3 are constants listed in Table A1.

- brine viscosity (Phillips et al., 1980):

$$\frac{\mu_b}{\mu_w} = 1 + am + bm^2 + cm^3 + d(T - 273.15)(1 - \exp(km)) \quad (21)$$

where T is the temperature in K, m is the molal concentration of equivalent NaCl in *g-moles NaCl/kg* H_2O, μ_b is the brine viscosity in *Pa.s*, and μ_w is the water viscosity in *Pa.s*:

$$\mu_w = \exp(C_1 + C_2/T + C_3\ln T + C_4T^{C_5}) \quad (22)$$

where T is the temperature in K. The constants of Eqs. (21) and (22) are equal to:

$a = 0.0816$, $b = 0.0122$, $c = 0.000128$, $d = 0.000629$, $k = -0.7$

$C_1 = -52.843$, $C_2 = 3703.6$, $C_3 = 5.866$,
$C_4 = -5.879e - 29$, $C_5 = 10$

brine electrical conductivity (Peyman et al., 2007):

$$\lambda_b = 0.096(T - 273.15)c - 0.8c^2 + 6.554c \quad (23)$$

where T is the temperature in K, c is the molar concentration of equivalent NaCl in *g-moles NaCl/Lit brine*, λ_b is the brine electrical conductivity in *S/m*.

- brine relative permittivity (Peyman et al., 2007):

$$\varepsilon'_b = \varepsilon'_w(0.999 + 8.521\times10^{-4}(T - 273.15)c + 0.013c^2 - 0.175c + 2.344\times10^{-4}(T - 273.15) - 1.235\times10^{-5}(T - 273.15)^2) \quad (24)$$

where T is the temperature in K, c is the molar concentration of equivalent NaCl in *g-moles NaCl/Lit brine*, ε'_b is the brine relative permittivity, and ε'_w is the water relative permittivity:

$$\varepsilon'_w = 10^{(1.94404 - 1.991\times10^{-3}(T - 273.15))} \quad (25)$$

where T is the temperature in K.

- oil density (Arnold and Stewart, 2008):
  The chart shown in Fig. A1 is used for calculating oil density.
- oil viscosity (Rossi et al., 2017):

$$\mu_o = 10^{-0.802.°API + 20.8765}(1.8T - 459.67)^{0.31458.°API - 9.21592} \quad (26)$$

where T is the temperature in K, and μ_o is the oil viscosity in *Pa.s*.

- oil electrical conductivity and relative permittivity:
  The relative permittivity and electrical conductivity of oil are both considered constant at 2.5e-8 S/m and 1.947e-11 F/m, respectively, because they change relatively little with temperature.

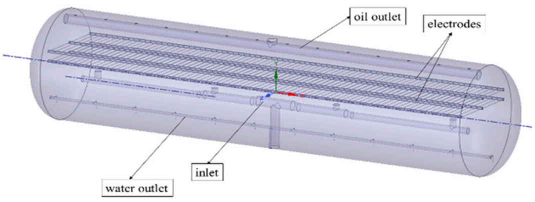

(a)

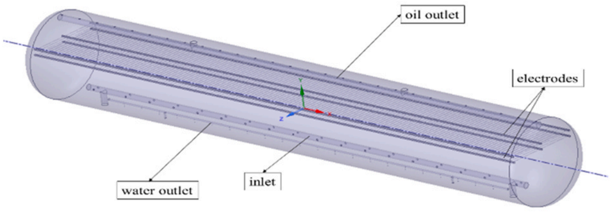

(b)

Fig. 1 – (a) RAD schematic, (b) IOFD schematic.

Table 2 – boundary conditions.

boundary	boundary condition: hydrodynamic	boundary condition: electrostatic
inlet	velocity inlet	$d\varphi/dx_i = 0V/m$
outlets	outflow	
walls	standard wall function	$\varphi = 0$ V
electrode connected to the ground		
electrode connected to the power supply		$\varphi = 32{,}000$ V

- interfacial tension (Ahmed, 2016):

$$\sigma' = 0.02 + 0.00003595(\rho_b - \rho_o) \tag{27}$$

where σ' is the interfacial tension in N/m, ρ_b and ρ_o is the brine and oil density in kg/m^3, respectively.

3.5. *Mesh independence study*

In this research, ICEM software is used to perform geometry gridding. The desalter geometry can be prepared with the different numbers of meshes for solving in ANSYS Fluent. A mesh independence study is carried out to guarantee the independence of ANSYS Fluent's solutions from the number of meshes. The results of this study for RAD case study are given in Table A2. It should be noted that in this study, the electric field is not applied to reduce computational costs.

As shown in Table A2, there is a significant difference in the chosen parameters as the number of meshes increases from 4.57 to 5.11 million. However, there is little difference between 5.11 million and 5.62 million, and between 5.62 million and 5.98 million meshes (less than 2%). Therefore, the use of 5.11 million meshes is considered for simulation in order to lower computational costs.

As the problems and equations solved by ANSYS Fluent in both cases (RAD and IOFD) are identical, the results obtained in the mesh independence study for the RAD can be applied in the IOFD. In both cases, the mesh size is considered the same. Therefore, the number of meshes for the IOFD in this scenario is 6.48 million.

3.6. *Class independence study*

Three cases with the number of 5, 10 and 15 classes are taken into consideration to ensure that the solutions are independent of the number of classes of brine droplets. The results of the class independence study are presented in Table A3. It should be noted that, like the mesh independence study, the electric field is not used to reduce the computational costs in this study.

As shown in Table A3, increasing the number of classes from 5 to 10 and 15 has no significant effect on the selected parameters. As a result, the remaining research steps are completed with 5 classes to reduce computational costs.

4. Results and discussion

4.1. *Validation*

The proposed method is compared with the Ramirez-Argaez et al. (2021) 's method (RAM). Two simulations with RAD geometry without an electric field are run to validate the proposed method in this study. In comparison, the results demonstrate that the volume average of the brine volume fraction in the whole system using the proposed method is 0.1002736, which is 0.25% different from the RAM value of 0.1000214.

To evaluate the performance of the electric field in the proposed method, the solutions in the absence and presence of the electric field are compared. The solution obtained in the presence of an electric field is then compared to the RAM solution.

The results show that the FAVFWOO has decreased from 0.0618 to 0.0304, i.e., 50.8%. Also, the maximum volume fraction of brine in the desalter has increased from 0.817 to 0.951, i.e., 16.4%. The changes in the separation and the maximum volume fraction of brine in the desalter can be seen in Fig. A2.

Fig. 2 depicts the number of droplets per unit volume of fluid (number density) in the presence and absence of an electric field. By comparing the number density, it is clear that the application of an electric field has a very clear effect on the decrease of the number density of droplets in the oil outlet indicating an increase in separation and sedimentation.

By comparing the results of the proposed method and RAM, it can be seen that FAVFWOO has significantly improved and lowered by 70%, going from 0.1 to 0.0304, demonstrating the proper efficiency of the proposed method. This is because using the population balance equation to simulate water droplets allows researchers to more thoroughly study the droplets' behavior. The reason for this difference is also due to how the population balance and the momentum equations take the effects of the electric field into account.

Table 3 – Operating conditions and physical properties at 120 °C and 10% wash water.

	RAD		IOFD	
	brine	oil	brine	oil
density (kg/m^3)	967.2	902.2	968.96	848.1
viscosity (Pa.s)	2.34e-4	0.0128	2.49e-4	0.0055
electrical conductivity (S/m)	2.94	2.5e-8	3.68	2.5e-8
absolute permittivity (F/m)	3.76e-10	1.947e-11	3.74e-10	1.947e-11
interfacial tension (N/m)	0.0223		0.0243	
crude oil flow at inlet (m^3/s)	0.1134		0.11	
salt (equivalent NaCl) mass flow rate at inlet (kg/s)	0.119		0.269	

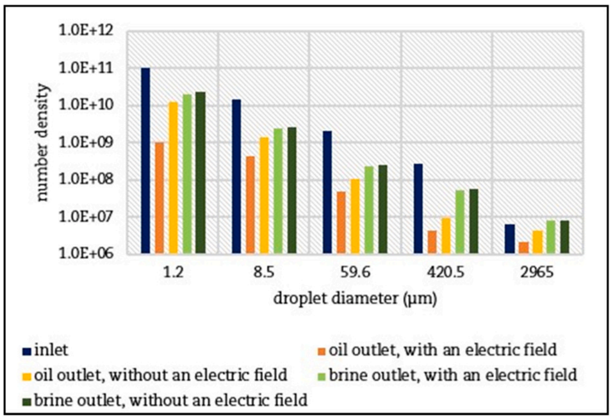

Fig. 2 – the number density of droplets.

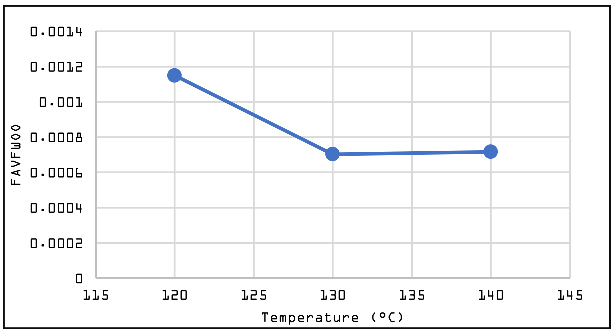

Fig. 3 – Changes in FAVFWOO vs. temperature.

4.2. *Sensitivity analysis for RAD case study*

By reviewing relevant references, it was found that the effect of temperature, the percentage of washing water, the inlet distributor, and the electrodes arrangement on the solutions can be investigated in the proposed method. As a result, a sensitivity analysis is performed on the mentioned parameters for the RAD geometry, which is a smaller model than the IOFD.

Eqs. (20) to (27) are added to the ANSYS Fluent software with UDFs to apply the effect of temperature on the physical properties of oil and brine. These functions call the temperature from the specified value inside the software.

The diagram in Fig. A3 is used to calculate the amount of remaining salt in the output oil. If the volume of the mixture brine is not 0.1%, the amount of PTB calculated from the chart is multiplied by the ratio of "mixture brine volume percentage to 0.1".

4.2.1. *Temperature*

The 120–140 °C temperature range is selected for sensitivity analysis (Abdel-Aal et al., 2003). Fig. 3 shows the FAVFWOO vs. temperature. By solving the problem at three temperatures of 120, 130, and 140 °C with 10% wash water, the FAVFWOO is 0.00115, 0.000703, and 0.000717, respectively and the salt content in the output oil is 5.35, 3.29, and 3.39 PTB, respectively.

The decrease in the FAVFWOO from 120° to 130°C is due to a decrease in oil viscosity, which allows brine droplets to separate more easily from oil. By increasing the temperature to 140 °C, a slight increase in the FAVFWOO is observed, which has reduced the brine density to the point where the effect of reducing the oil viscosity due to the reduced force of gravity on the brine droplets has been neutralized. Brine density and oil viscosity changes versus temperature are shown in Table A4. As seen in the table, the decrease in the brine density is greater than the oil viscosity. An increase in temperature over 140 °C also has an adverse effect on separation. It causes an increase in the FAVFWOO so that at a temperature of 160 °C, this parameter equals 0.0009.

4.2.2. *Wash water percentage*

By reviewing references, the wash water percentage range for the sensitivity analysis is set between 5 and 15 (Abdel-Aal et al., 2003). By solving the problem in three wash water volume percentages of 5, 10, and 15, with a temperature of 120 °C, the corresponding FAVFWOO is 0.00225, 0.00115, and 0.00041, respectively (Fig. 4), and the salt content in the output oil is correspondingly 21.85, 5.35 and 1.21 PTB.

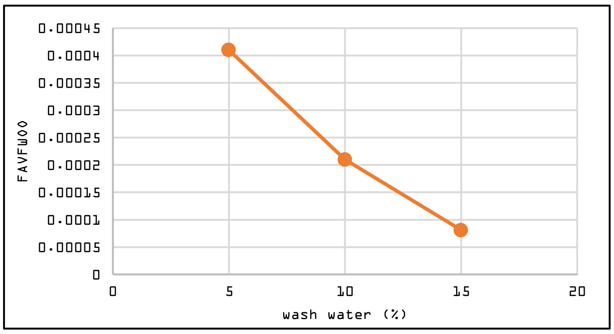

Fig. 4 – Changes in FAVFWOO vs. wash water percentage.

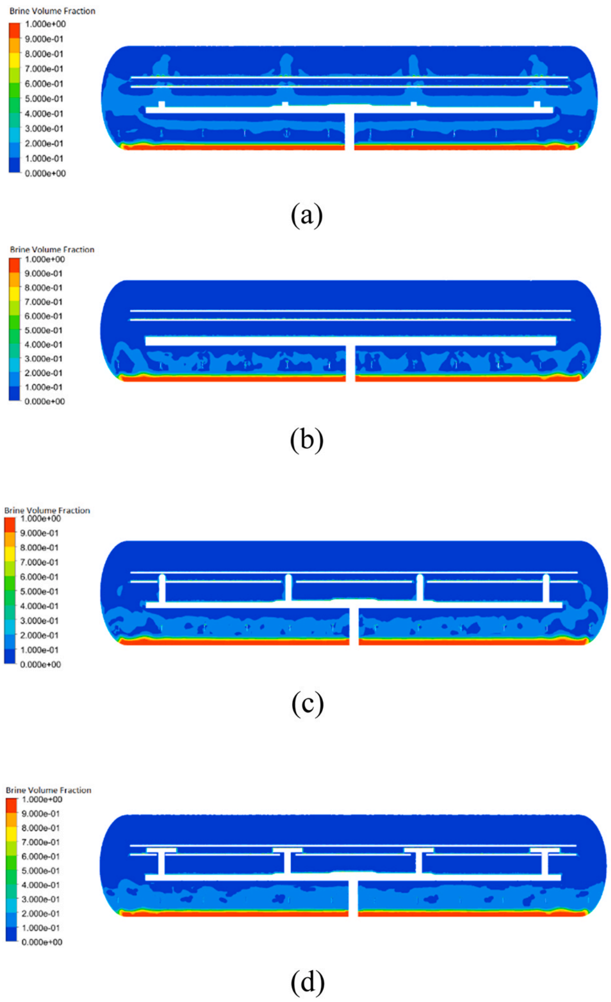

Fig. 5 – The brine volume fraction contour in different fluid distributions inside the desalter; (a) RAD Distribution; (b) Distribution along the desalter with a perforated pipe; (c) Distribution with perforated T-shaped pipes; (d) Circular distribution.

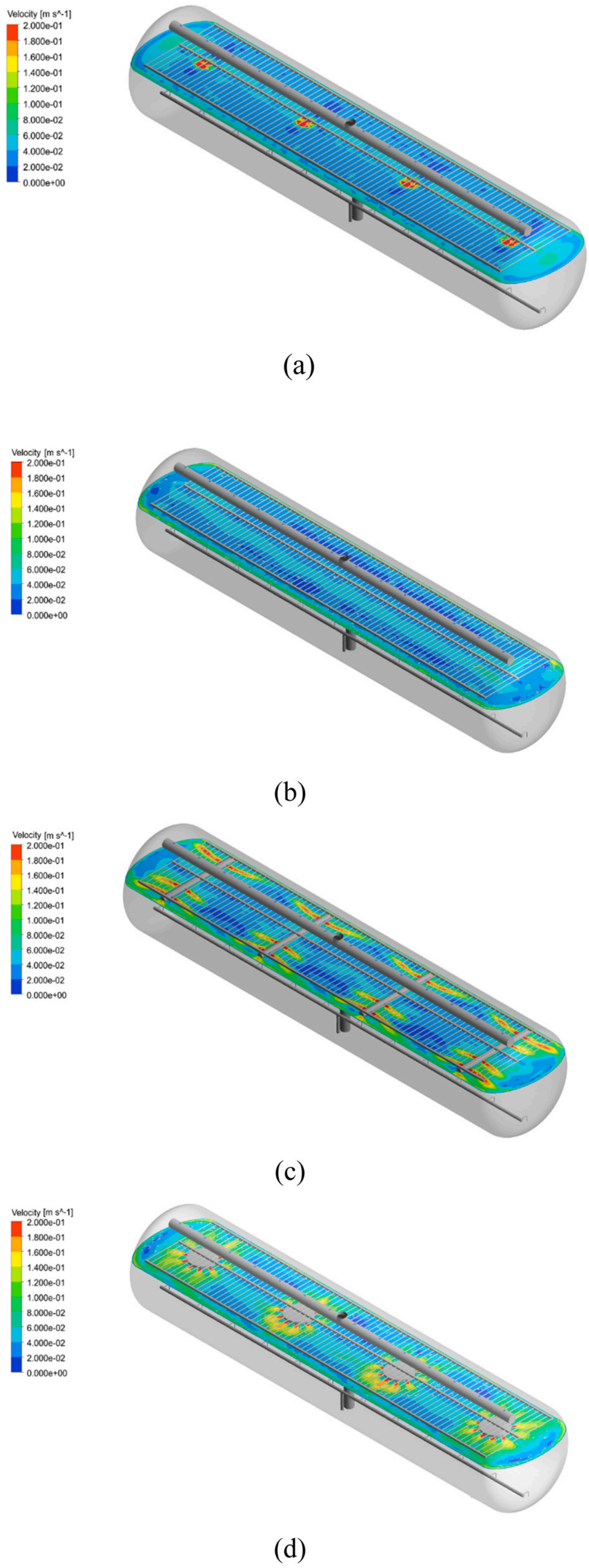

Fig. 6 – The velocity contour in different fluid distributions in the middle plane of the electrodes; (a) RAD Distribution; (b) Distribution along the desalter with a perforated pipe; (c) Distribution with perforated T-shaped pipes; (d) Circular distribution.

The increase in the number of brine droplets per unit volume has led to more droplets colliding with each other due to the application of an electric field, and the action of coalescence and sedimentation of brine droplets should be done more frequently. This is the cause of the decrease in the FAVFWOO with the increase in the wash water volume percentage.

4.2.3. *Inlet distributor arrangement*

The temperature and wash water percentage are set to 120 °C and 10, in this sensitivity analysis. Four different types of arrangements have been chosen. The first arrangement shown in Fig. 1(a) is related to the RAD geometry; Other arrangements are shown in Fig. A4. It should be noted that all inlet droplet size distribution is identical.

The FAVFWOO for the RAD and Fig. A4(a) to (c) distributions are equal to 0.00115, 0.00028, 0.00021, and 0.00048, and the salt

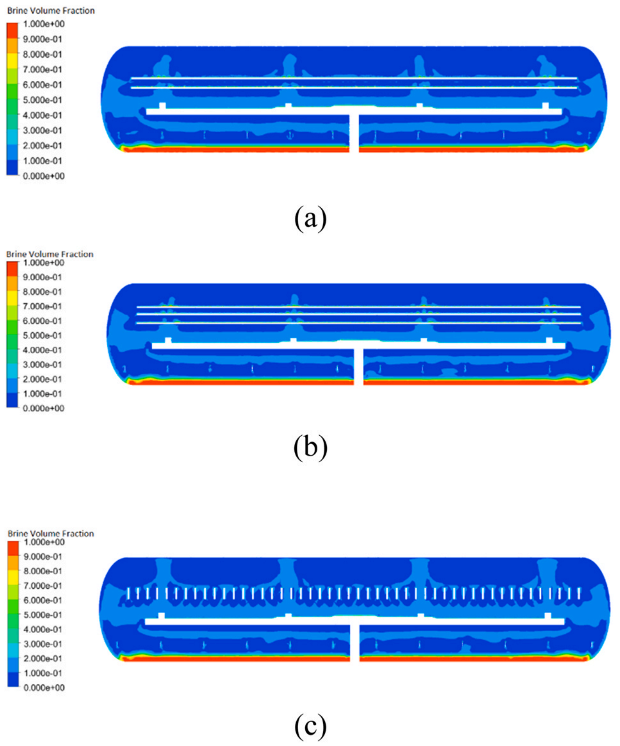

Fig. 7 – The brine volume fraction contour in different electrodes arrangement; (a) two horizontal electrodes; (b) Three horizontal electrodes; (c) Vertical electrodes.

content in the output oil is 5.35, 1.30, 0.98 and 2.23 PTB, respectively. These results are displayed in Fig. 5. As it is clear in Fig. 5, the separation in three distributions (b), (c), and (d) is evidently much better than distribution (a). As the FAVFWOO values in the three distributions (b), (c), and (d) are close to each other, Fig. 5 does not clearly show this difference.

According to the findings, when the distributor is changed, the separation rate alters significantly. As depicted in Fig. 6, this is due to a change in the distribution pattern of the mixture of oil and brine in the desalter. When using T-shaped pipes for distribution, the distribution is set up so that incoming flows collide most frequently at the entrance and in the middle of the electric field. This results in more droplet collisions, and separation will be improved.

4.2.4. *Electrodes arrangement*

The temperature and wash water percentage in this sensitivity analysis are 120 °C and 10, respectively. Three different types of arrangements have been chosen. The first arrangement is related to the RAD geometry, which is shown in Fig. 1(a); Other arrangements are shown in Fig. A5.

The FAVFWOO for the RAD and Fig. A5(a) to (b) arrangement is equal to 0.00115, 0.00098, and 0.02608, respectively, and the salt content in the oil output is 5.35, 4.56, and 121.33 PTB, respectively. These outcomes are displayed in Fig. 7. The separation in electrode arrangement (b) is better than that in electrode arrangements (a) and (c), as shown in Fig. 7.

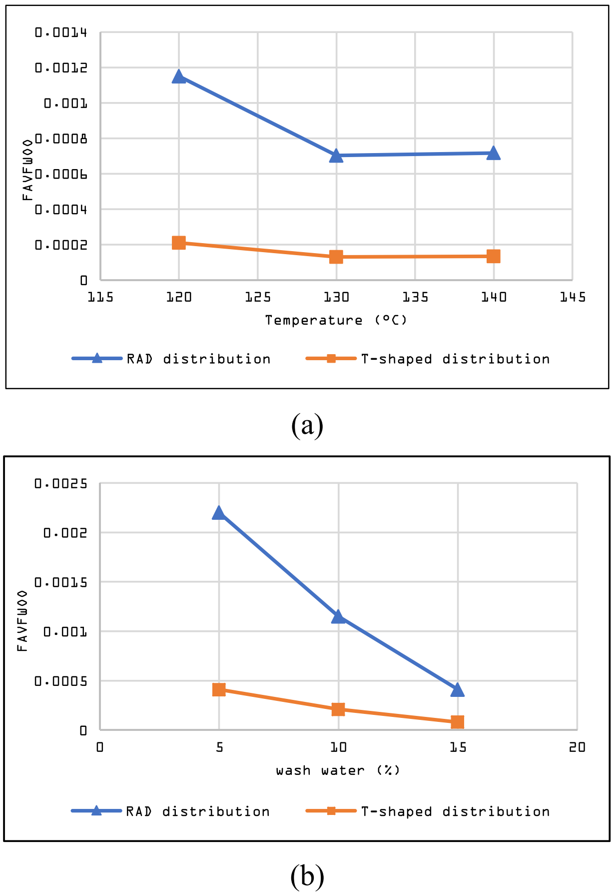

Fig. 8 – Comparison of FAVFWOO in RAD and T-shaped distributors.

Table 4 – IOFD sensitivity analysis results.

Temperature (°C)	wash water (%)	FAVFWOO	salt content (PTB)
90	5	0.00504	40.52
	8.3	0.00343	22.48
	10	0.00264	15.03
	15	0.00092	3.90
100	5	0.00349	28.26
	8.3	0.00244	16.09
	10	0.00188	10.77
	15	0.00066	2.79
110	5	0.00193	15.76
	8.3	0.00133	8.84
	10	0.00102	5.91
	15	0.00036	1.53
115	5	0.00116	9.49
	8.3	0.00080	5.35
	10	0.00061	3.50
	15	0.00023	0.99
120	5	0.00057	4.72
	8.3	0.00040	2.68
	10	0.00031	1.78
	15	0.00011	0.49

Additionally, electrode arrangement (c) has a lower separation than the others.

The findings indicate that increasing the number of horizontal electrodes from two to three, improves the separation by about 15%. The small change in separation in comparison to changing inlet distributor is caused by the fact that the electric field does not significantly change when going from two to three electrodes, as shown in Fig. A6(a) and (b).

To more precisely examine the effect of three horizontal electrodes on the output, the T-shaped distribution was chosen and the simulation was run at 120 °C and 10% wash water with three horizontal electrodes, yielding the FAVFWOO of 0.000206. When this result is compared to the result of the same case with two electrodes, it can be seen that increasing one electrode has improved the result by 1.9%, which is negligible when compared to the effect of changing the distributor. As a result, the change of electrodes is not taken into account in the study of IOFD.

4.2.5. *Interaction between parameters*

The simulation was run at temperatures of 120, 130, and 140 °C and 10% wash water in order to investigate the interaction of temperature with the inlet distributor. The FAVFWOO was calculated for the T-shaped distributor as 0.00021, 0.000130, and 0.000134, respectively. Fig. 8(a) compares the results with those obtained from the RAD distributor.

To investigate the interaction of wash water percentage with the inlet distributor, the T-shaped distributor was selected and the simulation was run at 5%, 10%, and 15% wash water and 120 °C. The FAVFWOO was obtained as 0.00041, 0.00021, and 0.00008, respectively. These results are compared with those obtained from the RAD distributor in Fig. 8(b).

Fig. 8 shows that both distributions exhibit a similar trend and percentage of the FAVFWOO changes. As a result, there is no interaction between the temperature and the inlet distributor, and between the wash water percentage and the inlet distributor.

4.3. *Sensitivity analysis for IOFD case study*

According to the process information of IOFD, the maximum brine in the output oil is 0.3 vol percent. For the IOFD, the temperature of 120, 130, and 140 °C was chosen like the RAD. After the simulation, the results showed that the FAVFWOO is within the acceptable limit. Then, by simulating the operating conditions mentioned in the process flow diagram namely the temperature of 115 °C and 8.3% wash water, it was found that the FAVFWOO is 0.0008, which is below the acceptable limit. For this reason and to save energy, the temperature of the simulation was reduced, and the simulation was run at temperatures of 110, 100, and 90 °C. The FAVFWOO is equal to 0.00133, 0.00244, and 0.00343, respectively. As can be seen, the acceptable limit has been rejected at a temperature of 90 °C. The simulation was run using a T-shaped distributor at this temperature and 8.3% wash water, and the FAVFWOO was 0.00255.

The temperatures for sensitivity analysis are taken to be 90, 100, 110, 115, and 120 °C based on the simulations. Furthermore, the wash water percentage is considered to be 5, 8.3, 10, and 15. For sensitivity analysis of temperature and wash water percentage in IOFD, the temperature was kept constant in the simulation and the percentage of washing water was altered. In this manner, 20 simulations were run, with the results shown in Table 4.

As shown in Table 4, the acceptable limit has not been met in the three cases of 90 °C and wash water percentage of 5 and 8.3, as well as 100 °C with wash water percentage of 5. In terms of temperature, 90 °C with 10% wash water is the best point for separation. While 100 °C with 8.3% wash water is the best point for separation in terms of wash water percentage. The cost of energy and wash water determines which of these two points is an optimal point.

5. Conclusion

In this study, the process of separating brine from oil in an electrostatic desalter was simulated using a combined method of CFD-PBM. ANSYS Fluent software was used to model the performance of electrostatic desalter. The mesh independence study and classes were done to find the optimal number of meshes and classes. The optimal number of meshes for RAD model was 5.11 million and for IOFD model was 6.48 million, and the optimal number of classes is 5. The results were compared with the RAD model to validate the method and there was only 0.25% difference. Finally, the sensitivity analysis of temperature, wash water percentage, inlet distributor arrangement, and electrodes arrangement were done for the RAD and the IOFD model. The results indicated that these four variables are independent to each other and the best inlet distributor arrangement is T-shaped and the number of two electrodes is the best arrangement. According to the results obtained from the sensitivity analysis in the IOFD model, the optimal point for separation in terms of temperature is 90 °C with 10% wash water. In comparison, the optimal point for separation in terms of wash water percentage was obtained at 100 °C with 8.3% wash water. Both suggestions can be applied to retrofit the desalter, depending on the energy and wash water costs.

Declaration of Competing Interest

The authors declare that they have no known competing financial interests or personal relationships that could have appeared to influence the work reported in this paper.

Appendix

See Tables A1-A4 and Figs. A1-A6.

Table A1 – Parameters for Eq. (20).

w/w% of equivalent NaCl	a_2	a_3
5	0.043	72.6
10	0.039	73.7
15	0.035	74.9
20	0.032	76.2
25	0.030	77.8

Table A2 – Mesh independence study results.

number of meshes	facet average of volume fraction of water at oil outlet (FAVFWOO)	facet average of velocity at oil outlet (m/s) (FAVOO)	facet average of velocity in the entire geometry (m/s) (FAVEG)
4571305	0.0664	1.6247	0.0295
5114144	0.0618	1.6830	0.0308
5618793	0.0610	1.6819	0.0302
5979832	0.0608	1.6904	0.0296
Error %	6.928	3.586	4.407
	1.294	0.066	1.948
	0.328	0.508	1.987

Table A3 – Class independence study results.

Number of classes	FAVFWOO	FAVOO	FAVEG
15	0.06110	1.68304	0.03099
10	0.06140	1.68302	0.03098
5	0.06180	1.68300	0.03080
Error % compared to 15 classes	-0.49100	0.00119	0.03227
	-1.14566	0.00238	0.61310

Table A4 – Brine density and oil viscosity changes versus temperature.

Temperature (°C)	brine density (kg/m^3)	oil viscosity (Pa.s)
120	942.6	0.0055
130	934.9	0.0047
140	926.8	0.0040
$\Delta_{120-130}$	7.7	0.0008
$\Delta_{130-140}$	8.1	0.0007

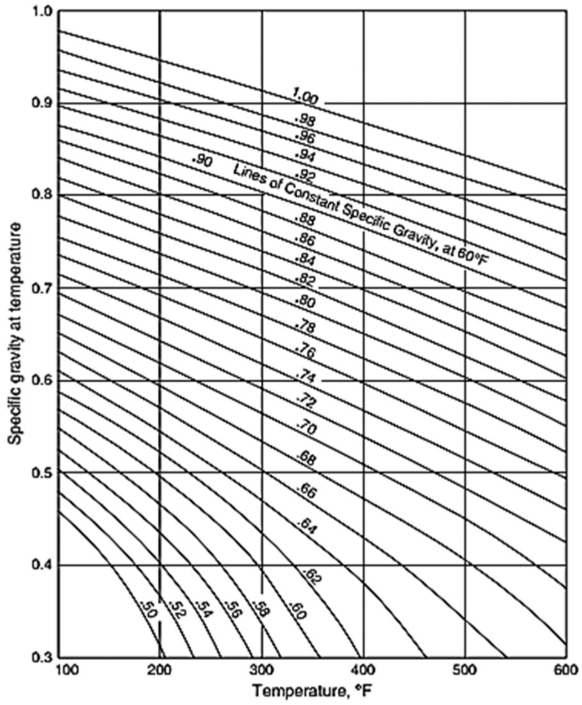

Fig. A1 – Chart of dead oil density Vs temperature (Arnold and Stewart, 2008).

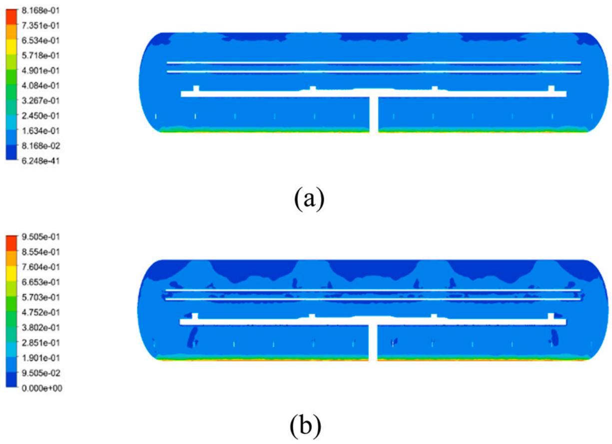

Fig. A2 – The contour of brine volume fraction in two states: (a) the absence of an electric field, and (b) the presence of an electric field.

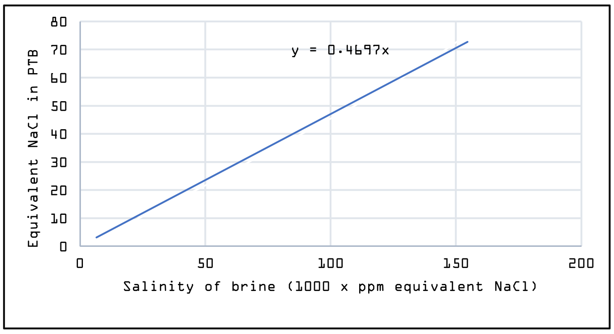

Fig. A3 – The salt content of crude oil (PTB) as a function of the salinity of its remnant - water 0.1% (1/1000) by volume of remnant water (Abdel-Aal et al., 2003).

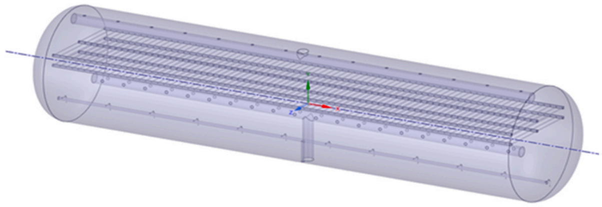

(a)

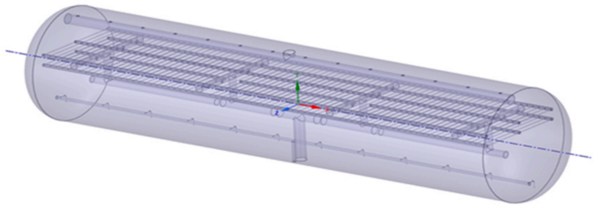

(b)

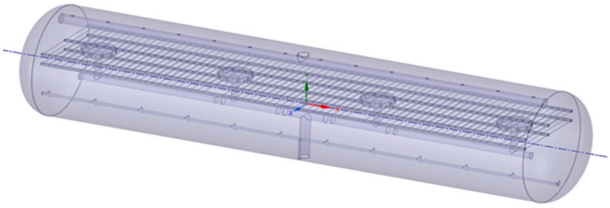

(c)

Fig. A4 – Desalter with different inlet distributor; (a) Distribution along the desalter with a perforated pipe; (b) Distribution with perforated T-shaped pipes; (c) Circular distribution.

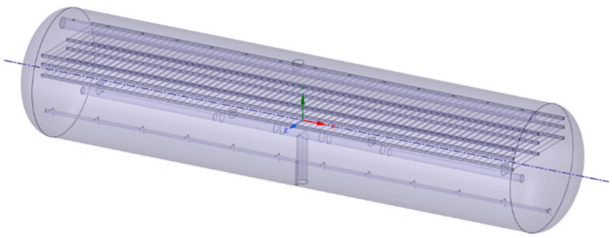

(a)

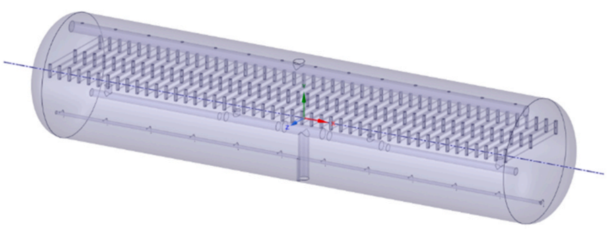

(b)

Fig. A5 – Desalter with different electrodes arrangement; (a) Three horizontal electrodes; (b) Vertical electrodes.

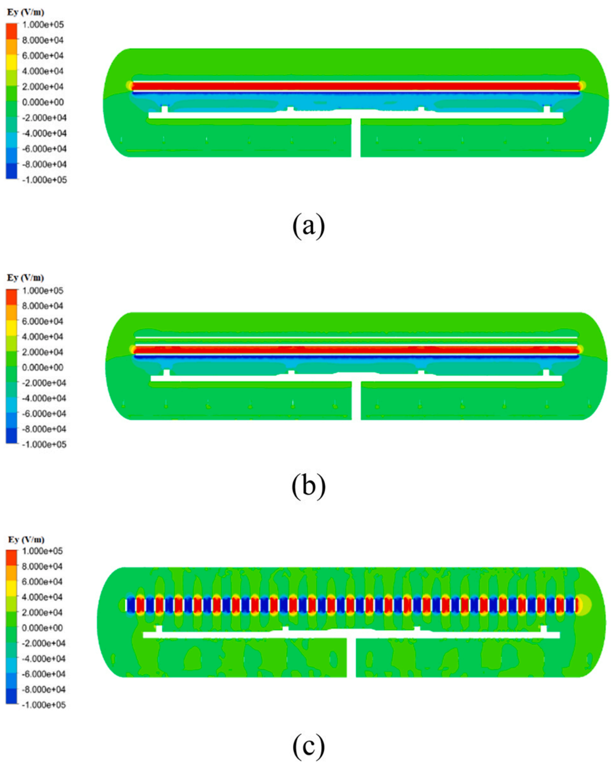

Fig. A6 – The contour of the y component of the electric field in different electrodes arrangement; (a) two horizontal electrodes; (b) Three horizontal electrodes; (c) Vertical electrodes.

References

Abdel-Aal, H.K., Aggour, M., Fahim, M.A., 2003. Petroleum and Gas Field Processing. Marcel Dekker, Inc, New York, USA, pp. 190–204. https://doi.org/10.1201/9780429258497

Ahmed, T., 2016. Equations of State and PVT Analysis: Applications for Improved Reservoir Modeling Ed. 2. Elsevier Science.

Al-Otaibi, M.B., Elkamel, A., Nassehi, V., Abdul-Wahab, S.A., 2005. A computational intelligence based approach for the analysis and optimization of a crude oil desalting and dehydration process. Energy Fuels 19 (6), 2526–2534. https://doi.org/10.1021/ef050132j

ANSYS, I., 2019. ANSYS Fluent Theory Guide.

Arnold, K., Stewart, M., 2008. Surface Production Operations Design of Oil Handling Systems and Facilities. Gulf Prof. https://doi.org/10.1016/B978-0-88415-822-6.X5000-4. Publ., Houst., US, pp. 440-441,.

Aryafard, E., Farsi, M., Rahimpour, M., Raeissi, S., 2016. Modeling electrostatic separation for dehydration and desalination of crude oil in an industrial two-stage desalting plant. J. Taiwan Inst. Chem. Eng. 58, 141–147. https://doi.org/10.1016/j.jtice.2015.06.028

Atten, P., 1993. Electrocoalescence of water droplets in an insulating liquid. J. Electrost. 30, 259–269. https://doi.org/10.1016/0304-3886(93)90080-Q

Dittman, G.L., 1977. Calculation of brine properties. Lawrence Livermore National Lab.(LLNL), Livermore, CA, USA. https://doi.org/10.2172/7111583

Gong, H., et al., 2021. Effects of droplet dynamic characteristics on the separation performance of a demulsification and dewatering device coupling electric and centrifugal fields. Sep. Purif. Technol. 257, 117905. https://doi.org/10.1016/j.jtice.2015.06.028

Kakhki, N.A., Farsi, M., Rahimpour, M., 2016. Effect of current frequency on crude oil dehydration in an industrial electrostatic coalescer. J. Taiwan Inst. Chem. Eng. 67, 1–10. https://doi.org/10.1016/j.jtice.2016.06.021

Khajehesamedini, A., Sadatshojaie, A., Parvasi, P., Rahimpour, M.R., Naserimojarad, M.M., 2018. Experimental and theoretical study of crude oil pretreatment using low-frequency ultrasonic waves. Ultrason. Sonochem. 48, 383–395. https://doi.org/10.1016/j.ultsonch.2018.05.032

Kiani, H., Moradi, S., Soulgani, B.S., Mousavian, S., 2013. Study of a crude oil desalting plant of the national iranian south oil company in Gachsaran by using artificial neural networks. Int. J. Environ. Ecol. Eng. 7 (12), 1015–1018. https://doi.org/10.5281/zenodo.1089573

Luo, H., Svendsen, H.F., 1996. Theoretical model for drop and bubble breakup in turbulent dispersions. AIChE J. 42 (5), 1225–1233. https://doi.org/10.1002/aic.690420505

Meidanshahi, V., Jahanmiri, A., Rahimpour, M.R., 2012. Modeling and optimization of two stage AC electrostatic desalter. Sep. Sci. Technol. 47 (1), 30–42. https://doi.org/10.1080/01496395.2011.614316

Oshinowo, L.M., Quintero, C.G., Vilagines, R.D., 2016. CFD and population balance modeling of crude oil emulsions in batch gravity separation—comparison to ultrasound experiments. J. Dispers. Sci. Technol. 37 (5), 665–675. https://doi.org/10.1080/01932691.2015.1054508

Oshinowo, L., Elsaadawy, E. and Vilagines, R., 2015. CFD modeling of oil-water separation efficiency in three-phase separators, 10th International Conference on Computational Fluid Dynamics in the Oil & Gas, Metallurgical and Process Industries. SINTEF Proceedings, pp. 207–216.

Peyman, A., Gabriel, C., Grant, E., 2007. Complex permittivity of sodium chloride solutions at microwave frequencies. Bioelectromagnetics: Journal of the Bioelectromagnetics Society, The Society for Physical Regulation in Biology and Medicine. Eur. Bioelectromagn. Assoc. 28 (4), 264–274. https://doi.org/10.1002/bem.20271

Phillips, S., Ozbek, H., Igbene, A., Litton, G., 1980. Viscosity of NaCl and other solutions up to 350 °C and 50 MPa pressures, California. University of California, Berkeley, USA. Lawrence Berkeley Lab.

Rahmat, A., 2017. Numerical Simulation of Multiphase Flows Under Electrohydrodynamics Effects., PhD Thesis, Sabanci University, Turkey.

Ramirez-Argaez, M.A., Abreú-López, D., Gracia-Fadrique, J., Dutta, A., 2021. Numerical study of electrostatic desalting process based on droplet collision time. Processes 9 (7), 1226. https://doi.org/10.3390/pr9071226
Roshan, N., Ghader, S., Rahimpour, M., 2017. Population balance equation modeling of crude oil demulsification considering demulsifier: modification of collision frequency function based on thermodynamic model. Int. J. Eng. 30 (10), 1434–1442. https://doi.org/10.5829/ije.2017.30.10a.03
Rossi, F., Colombo, S., Pierucci, S., Ranzi, E., Manenti, F., 2017. Upstream operations in the oil industry: rigorous modeling of an Electrostatic Coalescer. Engineering 3 (2), 220–231. https://doi.org/10.1016/J.ENG.2017.02.013
Sadatshojaie, A., Wood, D.A., Jokar, S.M., Rahimpour, M.R., 2021. Applying ultrasonic fields to separate water contained in medium-gravity crude oil emulsions and determining crude oil adhesion coefficients. Ultrason. Sonochem. 70, 105303. https://doi.org/10.1016/j.ultsonch.2020.105303
Tahouni, N., Abbasi, M., Panjeshahi, M.H., Eddine, M.R.N., 2023. Parametric optimization of a crude oil treatment unit to maximize oil production. Chem. Eng. Res. Des. 190, 20–32. https://doi.org/10.1016/j.cherd.2022.12.009
Thaker, A.H., Buwa, V.V., 2020. Separation of liquid–liquid dispersion in a batch settler: CFD-PBM simulations incorporating interfacial coalescence. AIChE J. 66 (11), e16983. https://doi.org/10.1002/aic.16983
Wang, T., Wang, J., Jin, Y., 2005. Theoretical prediction of flow regime transition in bubble columns by the population balance model. Chem. Eng. Sci. 60 (22), 6199–6209. https://doi.org/10.1016/j.ces.2005.04.027
Zeidani, K., Bahadori, A., 2008. New equations predicting the best performance of electrostatic desalter. Pet. Sci. Technol. 26 (1), 40–49. https://doi.org/10.1080/10916460600705634